Insights into microtubule catastrophes: the effect of end-binding proteins and force

Kalisch, S.M.J.

8 Final considerations and new research directions

This thesis gave a close-up view on microtubule catastrophes. We examined how forces and end-binding proteins affect the transition from growth to shrinkage. By using different methods ranging from quantitative and qualitative fluorescence intensity measurements to high-resolution optical tweezers experiments we targeted our research questions from different directions. Here we want to remark on our data and analysis and show preliminary observations connected to this topic. Besides, we present new research ideas emerging from our current experiments.

8.1 EB intensity

In order to understand the effect of end-binding proteins on microtubule (MT) dynamics we first examined the binding of the end-binding protein (EB) mal3 to MT ends, see chapter 3. We observed that mal3 intensity decreased on average several seconds before catastrophe which we explained with the disappearance of binding sites as a step towards catastrophe [Maurer et al., 2012]. While performing our experiments we identified three interesting future lines of investigations.

8.1.1 Mal3 intensity reflects the growth speed of MTs

Microtubule (MT) growth speed can be increased by elevating the mal3 concentration in the buffer (up to saturating conditions, ~200nM mal3) [Munteanu, 2008, Vitre et al., 2008]. This change of concentration is accompanied with an increased mal3 comet intensity, both in width and peak intensity of the comet [Munteanu, 2008]. As a result we wondered about a possible correlation between the instantaneous MT growth speed and the mal3 comet intensity. To clarify this issue we calculated the MT growth speed during each phase of free, constant growth. Next, we determined for each of these phases an average mal3 intensity (methods in chapter 3, page 105ff.). The resulting plot is shown in figure 8.1. To get a better overview we also grouped the intensities in speed intervals of same width and determined for each interval a time-weighted average. We see that with an increasing growth speed also the mal3 intensity increased, up to a growth speed of approximately 5 μm/min. Above this we cannot see a clear relationship which is possibly

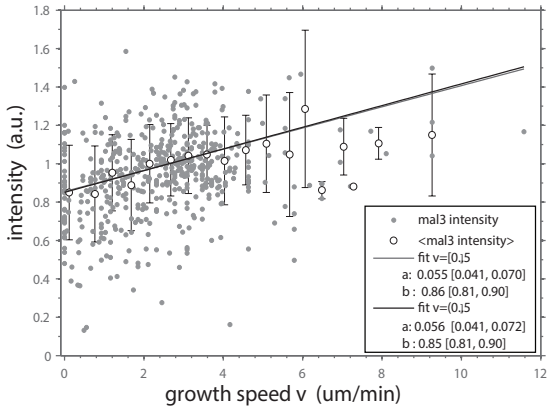

Figure 8.1: Mal3 intensity reflects the MT growth speed. For each interval during which the MT grew with constant speed we determined the average mal3-alexa488 intensity and MT growth speed (grey circles). We fitted the unbinned data with a linear function as first approximation, in the growth speed interval zero to 5 µm/min (grey line) and the same interval excluding zero (black line). For better view we grouped the data into intervals of constant width and determined for each interval a time-weighted average (open circles). The fit results are presented in the legend for a linear function y(x)=ax+b, with the 95 % confidence intervals in square brackets.

due to a saturation of the mal3 binding sites [Bieling et al., 2007, Munteanu, 2008] and also due to limited statistics. To quantify the relationship, we fitted the unbinned data, as a first approximation, with a linear fit. More precisely, we fitted in the range 0 to 5 µm/min and see a clear trend. We therefore suggest that growth speed is correlated with mal3 binding.

8.1.2 Correlated dynamics of end-binding proteins

To get a better picture of the regulatory effect of individual EBs we examined the correlated dynamics of mal3 and tip1 at MT ends. For analysis we proceeded as explained in section 3.2.2 with the difference of using mal3-mCherry and adding tea2 and tip1-GFP. Example kymographs are shown in figure 8.2a-c. The MT was not labelled for faster imaging purposes. As we could hence not identify the MT tip but only the EB comet, we could not exactly assess the instant of catastrophe. Instead, we defined by eye the time point when the tip1 intensity started reducing. As a consequence we also aligned the seventeen traces by the loss of the tip1 signal. As shown in figure 8.2d., both traces are similar to the one observed in the presence of only mal3 (fig. 3.5, page 31). Also here we observe a decrease of intensity, however it lasts only approximately 5 s. We believe that this results mainly from aligning the traces with the loss of tip1 signal instead of with catastrophe. Besides, all data stems from one single field of view and excludes therefore slight concentration and imaging differences. From the mal3 trace and previous results (chapter 3 and [Maurer et al., 2012]) we can estimate the moment of catastrophe to happen

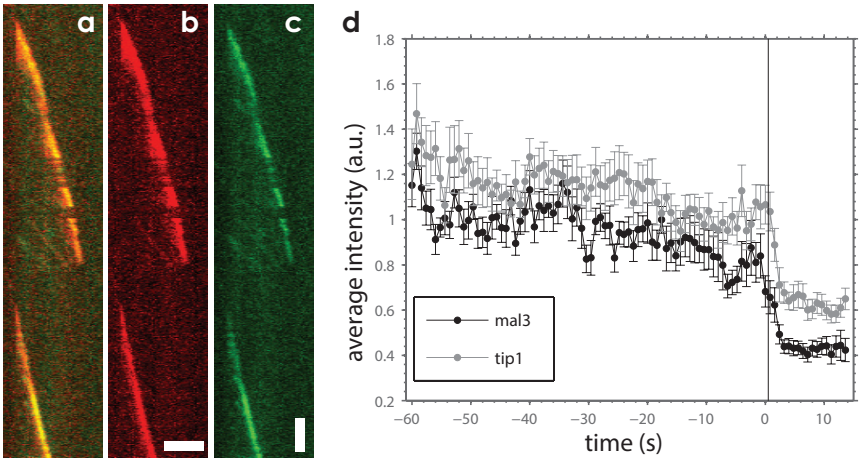

Figure 8.2: Protein intensities at MT ends during free growth. a. A colour-merge kymograph demonstrates a fluorescent mal3-mCherry and tip1-GFP comet at the tip of a dynamic MT. The MT grows from the seed and undergoes catastrophe which is accompanied by the loss of the EBs. Shortly afterwards, the MT renucleates from the seed. Vertical dark lines appearing abruptly in the comet are very likely caused by the MT being out of focus. They are not to be confused with a decreased affinity of the EBs to the MT tip. **b.** The same kymograph presenting only the mal3-mCherry signal and **c.** the tip1-GFP signal. Horizontal scale bar is 4 μm and the vertical one 25 s. **d.** We determined the maximum fluorescent intensity from a four-pixel long region at the MT tip. Here we show the average intensity, obtained from seventeen traces from one field of view, aligned at the sudden reduction of the tip1 signal (black vertical line). For the sake of faster imaging we did not label the MT fluorescently and could therefore not determine the exact time of catastrophe. Our data hence shows the tip1 binding dynamics with respect to mal3. On average, we observer the loss of mal3 followed by the one of tip1.

after the average mal3 intensity began decreasing. Interestingly, we see a small delay in the reduction of the tip1 signal compared to the mal3 signal (in the order of two seconds). We think that this is not solely caused by the delay in recording the two colours, which is here 0.3 s. Since tip1 and tea2 are thought to be able to proceed autonomously to the MT tip [Bieling et al., 2007], we also imagine that tip1 can bind directly to the MT tip and does not necessarily need mal3. This has also been shown experimentally for the tip1-homologue Clip170 [Bieling et al., 2008]. It was thought not to associate with with EB1 to the MT end, but to use a structural recognition mechanism. Since tip1 contains a structural domain which allows it to bind directly to α-tubulin we also suggest that tip1 recognises a structure at the MT tip rather than or besides binding directly to mal3. As explained, we envision mal3 to catalyse a structural change in the MT tip before catastrophe. The omission of this structure might also result in the loss of tip1 from the MT end. Why there remains the short delay in tip1 loss compared to mal3 loss remains to be elucidated. Possibilities are that the tip1-binding region is further away from the MT tip than is the mal3-binding region or that tea2/tip1 binding is not as critical to

the conformational state of the MT.

Our experiments only obtain information from the total EB intensity in the comet. One approach to learn more about the loss of mal3 (and/or tip1) from the MT end prior to catastrophe involves experiments with the same concentration of mal3 but a low fraction of labelled mal3. By doing single-molecule measurements at high time resolution we might be able to gain more information about the change of the MT comet. More precisely, we could learn about the change in width and length of the comet and also whether the mal3 binding region is different with respect to the one of tip1 or other end-binding proteins. Further, we might be able to deduce the internal dynamics in the comet such as whether mal3 unbinds from the MT tip or from the lattice end.

8.2 The catastrophe process

In chapters 4 and 5 we determined catastrophe time distributions of free MTs and those stalling at a barrier. We suggested catastrophes of free MTs to be comprised of two steps in the absence and presence of EBs with a longer step followed by a shorter one. Combined with the results from chapter 3 we proposed that the shorter step is characterised by the transformational change of the EB-competent state into the GDP-state.
MTs under force underwent a catastrophe faster than when there was no force present. Moreover, there was also a clear change when we added EBs: the histogram of catastrophe times shifted from a peaked multistep distribution to an exponential single-step one. Our explanation is that the force puts EB-decorated MTs immediately into the "ready-for-catastrophe" state where only one more event provokes transition to disassembly.
In the following we discuss our results and its implications on our view of MT assembly and disassembly.

8.2.1 Catastrophes: the underlying distribution

We fitted our data with four (truncated) probability density functions (pdfs):

- gamma distribution: consecutive steps have the same timescale
- two-step exponential distribution: two consecutive steps are not restricted to have the same timescale
- parallel two-step exponential distribution: two parallel/competing steps are not restricted to have the same timescale
- parallel multistep exponential distribution: parallel steps of equal timescale

In all of these distributions the steps are considered irreversible. Therefore we described a further distribution with the possibility of a backward step where an already performed step can be made undone. We did not fit our data with such a distribution since it contains more variables than we can deduce from our data. Here, however, we want to think about the consequences of such a process.

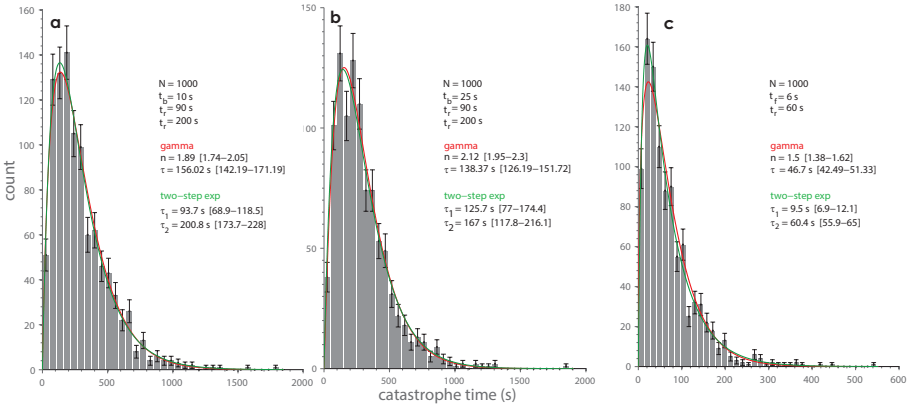

Figure 8.3: Simulated catastrophe time histograms for models introducing either a reversible step or a fixed-duration step. a-b. We assume a distribution describing a process with two random forward steps of duration t_r where the first step can be reversible with a timescale t_b. (A similar reaction with only irreversible forward steps is displayed in figure 4.5c.) The timescales for each step are presented by random numbers generated from an exponential distribution. **c.** This distribution is composed of a short, fixed step of duration t_f and a random long-term step of timescale t_r. Also here the random number was generated from an exponential distribution while the fixed-duration step was chosen. These generated or chosen numbers present the steps of the catastrophe process and were added up to obtain a catastrophe time, representing the duration of the total reaction (for a detailed explanation see section 8.3.2). Here we show the histograms of, in each case, thousand catastrophe times where the bin sizes are determined objectively [Freedman and Diaconis, 1981]. The unbinned data was fitted with gamma and two-step exponential distributions. The fit results are shown in the figure with the 95% confidence intervals in square brackets.

To get a better view of the consequences of a reversible process we simulated a distribution containing one backward step, see fig. 8.3a-b. These distributions, compared to our data obtained from free MTs in only tubulin (fig. 4.4a., page 41), display a wider peak and more apparent steps (gamma distribution), provided the backward step lasts longer than ten seconds. We can therefore not fully exclude a fast backward step in the catastrophe process. However, since in this case the reaction would be dominated by the longer forward steps the simplification to a two-step process is reasonable.

Common to all distributions is that the steps are thought to occur randomly. More specifically, the time point characterised by the transition from one state to the next takes place randomly. However, the assumption of random events does not necessarily need to be correct. It is also possible that one of the steps happens gradually. For example, assuming that after a first, random step the MT was in an intermediate state which immediately triggered the second step, the gradual transition to the final state. The second step would thus not occur randomly but would instantly follow the first step/transition. Further, it would always take the

same, fixed amount of time. An example of such a process is shown in figure 8.3c. Since this histogram resembles our data we cannot exclude the occurrence of a fixed, gradual step instead of a random one. Nevertheless, we can already say that the fixed step must be relatively short (a crude estimate yields half the bin width, so approximately 40 s for tubulin and 6 s for tubulin&EBs), otherwise we would not get a count in the first bin.

In this context we want to look at another problem, the different number of steps found for the catastrophe process. As already mentioned, Gardner et al [Gardner et al., 2011b] found approximately 2.5 - 3.4 steps until catastrophe, for free MTs grown in the presence of 7 - 14 μM tubulin (without EBs). This is larger than the ~1.8 steps we find. To understand the reason for the variation we analysed/repeated the experiments at different conditions (different tubulin batch (data of [Janson et al., 2003]), different conditions, 28° C, 12 μM tubulin and 110 mM KCl (same as [Gardner et al., 2011b])). The gamma distribution suggested 1.8 - 2.5 steps where the highest number of steps was found when using the conditions from [Gardner et al., 2011b] (data not shown). Whether the number of steps is changed by the experimental conditions, shows the inherent nature of the MT or stems from a simple systematic difference (e.g. surface blocking method) will be shown in the future.

8.2.2 The catastrophe process of MTs under force

Both for free MTs and MTs at a barrier we have a problem in accurately determining short events. For free MTs we solved this by fitting truncated distributions. However, at the barrier we would need more statistics to do this and to determine the precise number of steps. Nevertheless, our data clearly shows that the distributions for MTs under force (with tubulin / tubulin&EBs) differ while they look alike for free MTs. Whereas in the presence of force and tubulin we saw at least two steps, in the presence of force and EBs we only identified one. We suggested an explanation for the reduction of steps in the presence of EBs, namely the omission of the first catastrophe-promoting event. As we did not give a physical explanation for the increase of number of steps for MTs grown in only tubulin, let us look at this data in more detail now.

One putative scenario involves missing a short, third step for the free MTs. If this step lasted the same time for free MTs and for MTs at the barrier it could be retrieved at the barrier due to the relative duration compared to the other steps. To examine this we simulated three-step distributions, see fig. 8.4. Two steps were of similar timescales as obtained from our data of free MTs in the absence of EBs (here: t_{r1}=90 s and t_{r2}=210 s). A third fixed-duration step or a random step was added to the total catastrophe time. We fitted thousand such catastrophe times with gamma distributions and found that only for short third steps does the gamma distribution suggest less than two steps, as we found for our data. It seems that we hence did not miss a third step, unless it is faster than ~6 s (fixed)

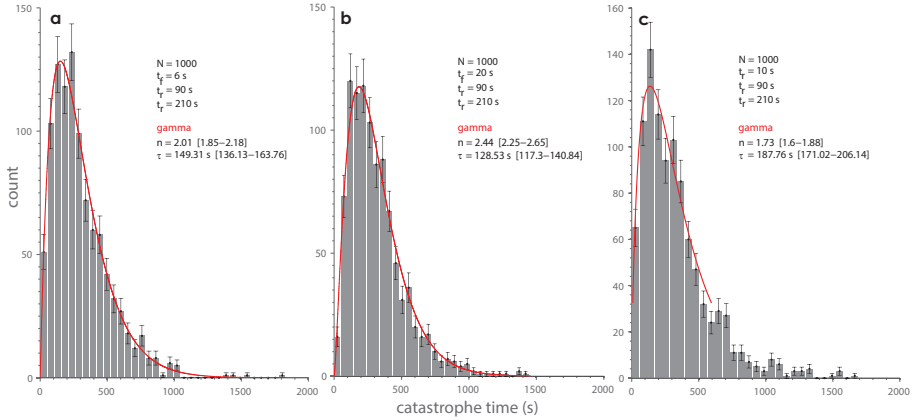

Figure 8.4: Simulated catastrophe time histograms testing the influence of a short step on the fitting parameters. Individual numbers were chosen (representing a fixed-duration step with timescale t_f) or random numbers were generated from an exponential distribution (representing a random step of timescale t_r). **a-b.** Two random numbers and one fixed one or **c.** three random numbers were added up to obtain a catastrophe time, representing the duration of the total reaction. Here we show the histograms of thousand catastrophe times where the bin sizes are determined objectively [Freedman and Diaconis, 1981]. The unbinned data was fitted with a gamma distribution where the fit results are displayed in the figure with the 95% confidence intervals in square brackets. The gamma distribution only suggests less than two steps if the third step is short. For our data, obtained in the absence of EBs, it means that we did not miss a third step, unless it is faster than ~6 s (fixed) or ~15 s (random).

or ~15 s (random). This teaches us that we cannot fully exclude a very short third step. Assuming therefore a three-step distribution for free MTs what would the distribution at the barrier look like? For this we simulated a process with N=1000 catastrophe times made up of two random steps and a third random or fixed one which was the shortest step and of ten seconds duration. Yet, no matter which combination we tried for the other two steps we could not reproduce our data at the barrier (data not shown). If the short step was comparably fast (the longer ones ~50 s) then the gamma distribution found only 2 to 2.5 steps (though we assumed three). This makes sense as the gamma distribution assumes steps of equal timescales which was not the case here. On the other hand, if two or all steps were comparably fast (all about 10 s long) then the gamma function found 3 to 4 steps. Yet, in this case the total reaction lasted much shorter than we measured for our data. We face comparable difficulties when simulating a distribution with four steps where one of them is of fixed duration, 10 s (data not shown). Conclusively, we do not think that we miss a step in the catastrophe process of free MTs which would show up at the barrier data. To understand the catastrophe process at the barrier more experiments are therefore necessary.

8.2.3 More insights into the catastrophe process

In line with the results of other studies we have found that the MT lifetime distribution does not follow an exponential decay but displays a clear maximum. As such, MTs that are already growing several minutes are more likely to catastrophe than freshly nucleated ones. In the literature this has led to the concept of "MT aging" which has also been observed through the gradual decrease of the EB comet intensity during steady-state growth [Maurer et al., 2012, Mohan et al., 2013]. For MT aging currently two main models exist.
In one of them MT aging not only refers to the time the MT has been growing but also to its accumulation of "defects" [Odde et al., 1995, Gardner et al., 2011b, Mohan et al., 2013]. Several ideas for these defects have been proposed. Kinetic steps could lead to transient states to which local and temporal criteria apply in order to render the MT instable [Brun et al., 2009]. Contrary, kinetic steps could lead to permament defects believing the MT to have a "memory" of them. A prominent example for such a catastrophe criterion is formed by the aforementioned GDP-terminated protofilaments with the condition of accumulating several such defects [Gardner et al., 2011b, Gardner et al., 2013]. Recent studies have indeed shown that GDP-tubulin at the MT end has an impact on further growth [Piedra et al., 2016, Kim and Rice, 2019, Cleary and Hancock, 2021]. Furthermore, calculations based on the catastrophe criterion of accumulating three such defect protofilaments well agreed with experimental results and MT lifetime distributions [Bowne-Anderson et al., 2013].
On the other hand, an analytic extension of these calculations and a fit to MT delay times after tubulin washout experiments failed to fit or implied rate constants that contradict experimental data [Duellberg et al., 2016b]. In addition, *in vitro* TIRF experiments with two differently coloured tubulin dimers showed that laser-induced MTs can repair themselves, leading to quite stable rescue-inducing lattice sites [Aumeier et al., 2016]. As we have shown, EBs are highly capable of influencing MT stability by e.g. mal3 inducing a compaction of the lattice [Maurer et al., 2012], XMAP215 binding and removing tubulin dimers from the MT end [Brouhard et al., 2008] or CLASP stabilizing incomplete lattices [Aher et al., 2018, Mahserejian et al., 2022]. In *in vivo* environments where these microtubule-associated proteins, among others, are present it is hard to imagine that a MT could not "repair" a GDP-capped protofilament and render it capable of further growth. This holds especially in the light that also cells are found to repair damaged MT lattices [Aumeier et al., 2016] and that further experiments with TIRF microscopy and Monte Carlo modelling have shown that the MT lattice can rejuvenate itself [Schaedel et al., 2019].
Also in this thesis we have analyzed our data based on the assumption of the multistep defect model. We have found no cue as to decide whether these steps are transient or permanent and what the molecular nature of these steps could be. Confirming this problem, todate experiments are missing which give a deeper molecular insight into the multistep catastrophe model. It does not make it easier that also the mechanism of growth leaves many questions open and the postulated

conditions for MT catastrophe cannot be probed directly.

Next to the defect-accumulation model for explaining the peaked MT lifetime distributions is the "taper-cap density" model. Electron microscopy images had shown rugged extensions at the microtubule ends indicating that not all protofilaments have the same length [Mandelkow et al., 1991, Chretien et al., 1995]. These so-called tapered tips are found increasingly pointed over the MT lifetime causing progressive instability [Coombes et al., 2013]. Duellberg at al. assumed in their MT washout experiments [Duellberg et al., 2016a] that MT destabilization occurs by lattice maturation (through random hydrolysis and accompanying conformational changes) and slow depolymerization (by the ongoing dissociation of tubulin subunits after free tubulin washout) until a critical density is reached. Catastrophe occurs when this critical density is reached at the very end of the blunt MT. Taking into account a tapered MT end changes the density of binding sites in the MT: the more tapered the MT becomes, the more the binding sites are distributed and the lower the density of binding sites becomes. Thus, an "older" MT with already a lower density of binding sites at steady state reaches the critical density threshold faster than a MT which "starts" with a higher density at washout [Duellberg et al., 2016b].

Next to these two lines of reasoning several MT growth and catastrophe models exist explaining experimental data without these two MT aging models. Assuming different hydrolysis mechanisms (vectorial, random or coupled or often a combination of these) often in conjunction with different tubulin dimer association rates depending on longitudinal and lateral protofilament interactions in the 3D MT lattice results in a multitude of models fitting data with more or less varying accuracy [Margolin et al., 2012, VanBuren et al., 2002, Gardner et al., 2011b, Mickolajczyk et al., 2019, Bowne-Anderson et al., 2013, Coombes et al., 2013]. Also our model of fluctuating tip growth, random hydrolsysis in a 1D MT lattice, together with a critical density as a catastrophe criterion, can explain a range of experimental data including washout experiments, see chapter 7. Here, the progressive increase of the catastrophe probability over time is reached by introducing a time-dependent, increasing tip (growth) noise, gradually raising the probability for an unstable MT tip.

At the moment, it is not clear which of the above mentioned models is really describing MT dynamics and further investigations are crucial. At the moment the dilemma between low resolution and dynamic imaging methods (light microscopy) versus high resolution but static ones (electron microscopy) poses a limit. Only with new ideas will our horizon be broadened.

8.3 High resolution on MT growth under force

In chapter 6 we examined the influence of force on the MT growth speed using optical tweezers. Though free MTs grow faster in the presence of mal3, tea2 and

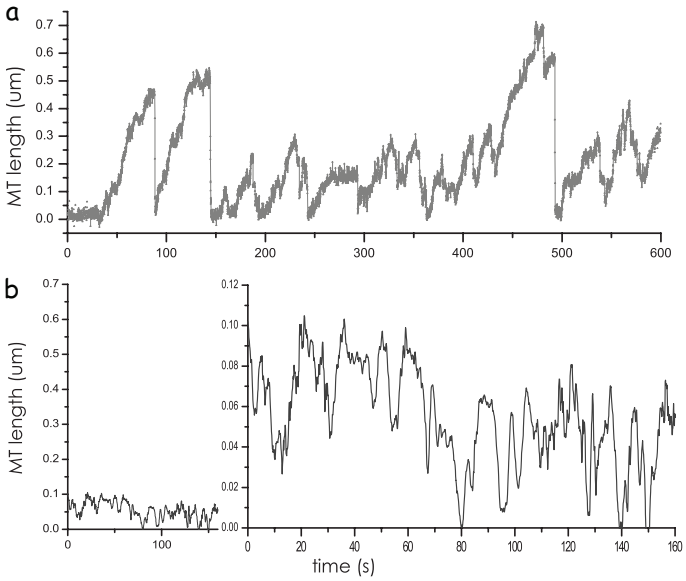

Figure 8.5: MT growth traces obtained with optical tweezers. MTs are grown from a bead-axoneme construct against a rigid barrier. MT growth results in displacement of the trapped bead from which we can deduce the MT length. Here, MT length is plotted over time in the presence of tubulin with mal3, tea2 and tip1. **a.** This example shows twice the nucleation of a single MT after which only MT bundles are nucleated. **b.** We occasionally saw repeated "saw-tooth" growth events where MTs do not grow long and have frequent catastrophes and (re-)nucleation events. In the presence of tubulin alone we never observed this type of dynamics. The *right* figure shows the same data as on the *left*, zoomed in.

tip1 than in their absence, we could not observe this under force. We explained this result with our aforementioned observation about the loss of the mal3 comet under force. Since mal3 may unbind from the MT already at small forces we think that the effect of EBs on MT growth speed is only visible for forces F< 0.5 pN. Thereafter the MT tip is not bound by EBs even if they are present in the buffer and the growth speed is (almost) the same as for MTs grown in pure tubulin.

8.3.1 Growth at small forces

The interesting questions thus are: do EBs affect MT growth only at small forces, F<0.5 pN ? If yes, of what nature is the force-growth speed relationship in this case ? For this we would need to measure at forces smaller than 0.5 pN. This could be tried with the use of force-feedback though it is experimentally hard. Another, easier, method is to analyse our data carefully in the "soft-regime". At the barrier MT growth does initially not result in displacement of the attached bead from the trap centre. The reason is the elastic unspecific attachment between bead

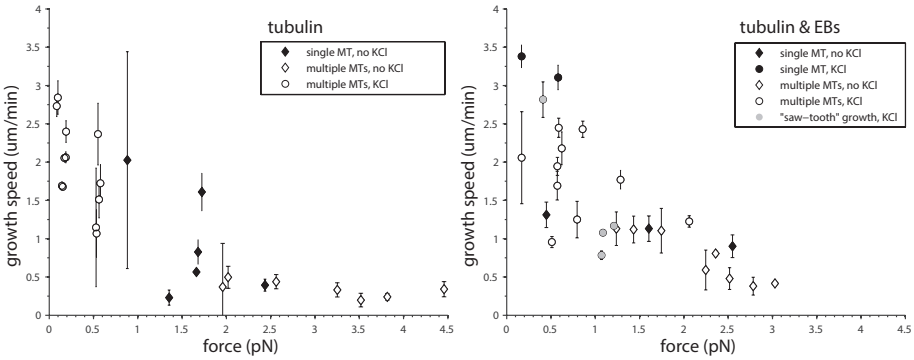

Figure 8.6: Force - growth speed relationship of "saw-tooth" growth. Average growth speed and average force for MTs grown in different conditions (left in pure tubulin, right in presence of tubulin and mal3, tea2 and tip1; open symbols: multiple MTs, black symbols: single MTs, grey symbols: "saw-tooth" growth; diamonds: no added salt, circles: 50 mM KCl added). Considering force generation and growth speed saw-tooth growth is comparable to "normal" MT growth events. (This figure is adapted from fig. 6.5.)

and axoneme. Only after this attachment is stretched out, after about 50 nm, is MT length proportional to the bead displacement (see page 68ff.). Since here it is easier to deduce force and MT length we measured only in this regime. With careful analysis we can also analyse the MT growth trajectories in the presence of EBs at the initial build-up of force.
Another complication of the experiment is the nucleation of multiple MTs. Since they can share the force load and it is hard to determine the exact number of MTs it is hard to reliably reproduce and analyse such data. As the nucleation of several MTs happens far more often in the presence of EBs than in their absence it makes the comparison between the two datasets difficult. This also obstructs the effect of EBs on the MT growth speed. Therefore a better control of MT nucleation, e.g. by altering the tubulin concentration or the temperature would improve our insight into effect of EBs.

8.3.2 "Saw-tooth" growth dynamics

In the presence of EBs we occasionally saw repeated catastrophe and (re-) nucleation cycles during which MTs stayed relatively short (< 0.3 µm), see figure 8.5. Growth occurred in short bursts and the MT did not shrink back to the axoneme but experienced many "rescue" events. We rarely observed this "saw-tooth" growth pattern in the presence of pure tubulin and therefore find mal3, tea2 and/or tip1 responsible. Comparing figure 8.5a and b (left), we can be sure that saw-tooth growth is not noise. On the other hand, it is also not representing an artifact since after some time of saw-tooth growth the MT usually nucleated a "normal" growth event. We observed that the nucleation of one/the first MT under force in the presence of

EBs is difficult and therefore fewer MTs are nucleated. This is opposite to the case of free MTs were EBs increase the nucleation frequency of MTs. To increase the occurrence of nucleation we placed the axoneme tip approximately 50 nm in front of the barrier such that only after having grown to a length of 50 nm the MT would experience a force. Conclusively, we can say that MTs with EBs have difficulties in nucleation under force and therefore display this saw-tooth dynamics. We surmise that it represents tubulin structures not yet closed into the MT tube. The results of a first analysis analogously to described in chapter 6 are presented in figure 8.6. Nonetheless, it might be useful to analyse their dynamics in detail which might give us useful information about the structural effects of EBs of MTs under force.

Methods

Here we will only remark on the differences to the more extended explanation of methods in the respective chapters.
To measure the correlated dynamics of EBs we used both labelled mal3-mCherry and tip1-GFP and unlabelled tea2. The microtubule was not fluorescent, however, the seed contained tubulin-HiLyte635. We measured at time-lapse intervals of 0.8 s.
For the simulation of a reversible-step distribution we generated N=1000 catastrophe times, each comprised of two forward, random steps of duration τ_1 and τ_2. We then added another random backward and forward step (of duration τ_{-1} and τ_1, respectively) to τ_1/τ_{-1} N catastrophe times. This represents the reversibility of the first reaction occurring once. Since a backward reaction could possibly occur more often, we added a second forward and backward step to $(\tau_1/\tau_{-1})^2$ N catastrophe times. The probability for a further backward step is so small that we omitted it.

Acknowledgements

I want to thank Olga Sytina for help in preparing the optical tweezer experiments, for carrying them out and for doing most of the optical tweezers data analysis. Further, I want to thank Katja Zieske for performing the correlated intensity experiments containing mal3-mCherry and tip1-GFP. I am grateful that Magdalena Preciado-Lopez performed the experiments of free MTs grown in 12 μM tubulin at 28° C.
We thank Chris Rétif, Gijs Vollenbroek and Hans Zeijlemaker for their advice on micro-fabrication, E. Laura Munteanu, and Julien Husson for help with the optical trap assay and Roland Dries for developing the bead-tracking software. We appreciate the generous axoneme present from Matt Footer. We are grateful for the help of Peter Bieling and Thomas Surrey with the protein purification of mal3-alexa488, tea2 and tip1 and for generously providing us a mal3-GFP vector.
The work presented in this chapter was carried out as part of the EU Program AMOCROSS, as part of a "VICI" grant provided by the "Nederlandse Organisatie voor Wetenschappelijk Onderzoek (NWO)" and as part of the research program of the "Stichting voor Fundamenteel Onderzoek der Materie (FOM)", which is financially supported by the "Nederlandse Organisatie voor Wetenschappelijk Onderzoek (NWO).